第 48 卷 第 2 期
2021 年 2 月

湖南大学学报（自然科学版）
Journal of Hunan University（Natural Sciences）

Vol. 48. No. 2.
Feb. 2021

Open Access Article

Automatic Filler Dispersion Quantification in Microstructure Images of Bottom Ash Reinforced Polymer Composite

Fajar Astuti Hermawati[1], I Made Kastiawan[2], Muhyin[2]

[1] Department of Informatics, Universitas 17 Agustus 1945 Surabaya, Indonesia

[2] Department of Mechanical Engineering, Universitas 17 Agustus 1945 Surabaya, Indonesia

Abstract: Distribution or dispersion analysis of polymer composite particle fillers is crucial to determine the material's properties and strengths. Bottom ash was used as reinforcement particles in the polymer composite. Bottom ash particles have an irregular shape, porous structure, and rough texture surface. The characteristics cause difficulty in detecting and analyzing the particles in the microstructure image of the polymer composite. This study aimed to build a robust method to detect bottom ash particles in the polymer composite automatically through microstructure image observation. The proposed method can also identify the agglomerated bottom ash particles, separate them, and analyze the distribution. Firstly, an image enhancement technique is applied to eliminate noise in the input image. A multi-level fuzzy segmentation method is implemented to obtain the filler particles region. Each particle region obtained is examined whether it is a touching particle and split it using an edge detection-based method. Before implementing the edge detection, the void filler algorithm is applied. We used a Prewitt edge detector that combines filling gaps between two broken segments using a round mask. The logic difference operation between the whole area and the resulting edge area is implemented to separate the touching particle region. At finally, the quantification of filler dispersion is carried out. To investigate the performance of the splitting method, we compared it with the watershed method. In experiments, this touching particle splitting method can separate agglomeration particles with more than 90% accuracy. This study has two-fold novelties. Firstly, this pioneering study automatically identifies and quantifies filler particles with irregular shapes using image processing techniques. Second, the proposed splitting method has better performance than the watershed method used in previous studies.

Keywords: image processing, dispersion analysis, bottom ash particles, agglomeration particle, microstructure image.

底灰增强聚合物复合材料微观结构图像中填料的自动分散定量

抽象:

聚合物复合颗粒填料的分布或分散分析对于确定材料的性能和强度至关重要。底灰用作聚合物复合材料中的增强颗粒。底灰颗粒具有不规则形状，多孔结构和粗糙的表面纹理。该特性导致难以检测和分析聚合物复合物的微结构图像中的颗粒。这项研究旨在建立一种可靠的方法，通过微观结构图像观察来自动检测聚合物复合物中的底灰颗粒。所提出的方法还可以识别附聚的底灰颗粒，将其分离，并分析其分布。首先，应用图像增强技术来消除输入图像中的噪声。实现了一种多级模糊分割的方法来获得填料颗粒区域。检查所获得的每个粒子区域是否为接触粒子，并使用基于边缘检测的方法对其进行分割。在实施边缘检测之前，应应用空隙填充算法。我们使用了普威特边缘检测器，该检测器使用圆形蒙版组合了两个破碎段之间的填充间隙。整个区域与所得边缘区域之间的逻辑差运算被实现为分离触摸粒子区域。最

Received: 7 January 2021 / Revised: 14 January 2021 / Accepted: 12 February 2021 / Published: 28 February 2021

Fund Project: Research grant PTUPT DRPM Direktorat Jenderal Riset dan Pengembangan Kementerian Riset, Teknologi, dan Pendidikan Tinggi, Indonesia.

About the authors: Fajar Astuti Hermawati, Department of Informatics, Universitas 17 Agustus 1945 Surabaya, Surabaya, Indonesia; I Made Kastiawan, Muhyin, Department of Mechanical Engineering, Universitas 17 Agustus 1945 Surabaya, Surabaya, Indonesia

Corresponding author Fajar Astuti Hermawati, fajarastuti@untag-sby.ac.id

后，进行填料分散的定量。为了研究分割方法的性能，我们将其与分水岭方法进行了比较。在实验中，这种接触式颗粒分裂方法可以以90％以上的精度分离附聚颗粒。这项研究有两个新颖之处。首先，这项开创性研究使用图像处理技术自动识别和量化了具有不规则形状的填料颗粒。其次，所提出的分裂方法比以前的研究中使用的分水岭方法具有更好的性能。

关键词: 图像处理，色散分析，底灰颗粒，团聚颗粒，微观结构图像。

1. Introduction

Composites can be defined as materials consisting of two or more phases that are chemically and physically separated by different interfaces [1]. The behavior of composite materials is explained based on the combined action of the reinforcing elements, polymer matrix, and fiber or matrix interface. To achieve superior mechanical properties, the interface adhesion must be strong. Matrix molecules can be anchored to the fiber's surface by chemical reaction or adsorption, determining interfacial adhesion level. The interface investigation was conducted through microstructure images obtained using electron microscope devices such as a Scanning Electron Microscope (SEM) and Transmission Electron Microscope (TEM) or optical microscope devices the digital microscope.

Dispersion analysis to determine the distribution of reinforcing particles is essential to underlie the measurement of polymer composites' mechanical properties [2–8]. The more evenly distributed the particles of filler, the stronger the material produced. Bottom ash is one of the polymer matrix fillers which has the advantage of having a rough surface, and the shape is not homogeneous. Moreover, bottom-ash particles have a large pore structure, so that it is a reason to enlarge the adhesive bond [9–11]. On the other hand, due to the irregular shape of bottom ash particles, analyzing these particles' dispersion in microstructure images is not easy and requires robust segmentation techniques.

To get the distribution of filler particles in the polymer matrix, we need to detect each particle's presence in the polymer matrix layer both in the direction and perpendicular direction of the observation field. The problem is for the clumping particles or overlapping particles. We have to split the clumping particles so that we can detect each particle in the cluster. Some segmentation studies for separating the overlapping objects implement the watershed method [12–17]. Nevertheless, the researchers apply the watershed technique to segment objects with regular shapes such as circles or ellipse.

In this study, we propose an automatic filler particles distribution analyzer that processes a microstructure image of polymer composite and results in a distribution index of filler particles in the image. Firstly, we implement an image enhancement method to improve the quality of the image. The enhancement technique uses the hybrid approach that combines Wavelet multiscale algorithm and spatial filtering method. The advantage of this approach can reduce noise while preserving the image detail components [18]. Furthermore, to obtain the particle regions in the image, a Fuzzy based multi-level thresholding method is applied. According to Sarkar et al. [19] and confirmed by the research of Naidu et al. [20], fuzzy-based entropy has better performance than the Shannon entropy approach. For each particle region obtained from the segmentation step, we separate the overlapping particle using edge detection-based segmentation techniques instead of region-based segmentation. Several techniques get the object's edge, such as the active contour method [21] and edge detection with operators. The weakness of active contour is that it requires an extensive iteration so that the computation time required is also considerable. In this research, edge detection is used to get the boundary between overlapping objects. The gap-filling is applied to connect the disconnected edges. Individually, the splitting method was tested using overlapping particle images, and it was measured quantitatively by region-based performance measurement. The performance of the proposed segmentation method was also compared to the watershed method. Finally, we calculate the distribution index of filler particles in the whole image using a Gaussian probability density function based on the particle region center [8]. When compared with the automatic index dispersion calculation system that was proposed by Li et al. [8], our entire pipeline for filler particle dispersion analysis can detect particles that are not uniform in size and separate touching and overlapping particles. The precision of measuring the distribution of filler particles in the composite polymer becomes better.

Our main contribution is developing an automatic technique to quantize filler particles' distribution with non-uniform sizes and irregular shapes. It will help analyze the strength of the material by measuring the particle distribution quickly and precisely. We also propose a method for recognizing and splitting agglomerated particles to support the automatic filler dispersion system's robustness.

This article is organized into several sections. After

the introductory part, the first section is the research methodology that discusses the proposed segmentation methods. The results and discussion are explained in the second section. This section evaluates the proposed method's performance and the comparison method. The last section consists of conclusions and suggestions.

2. Research Methodology

The proposed method is fully described based on Fig. 1. The main steps of this filler particle dispersion analyzer consist of the image quality improvement step to improve the detection accuracy of the particle area, the segmentation of the particle area from the polymer matrix, the detecting and separating the accumulated or agglomerated particle areas, and the stage of calculating the distribution index or the dispersion index of the filler particles.

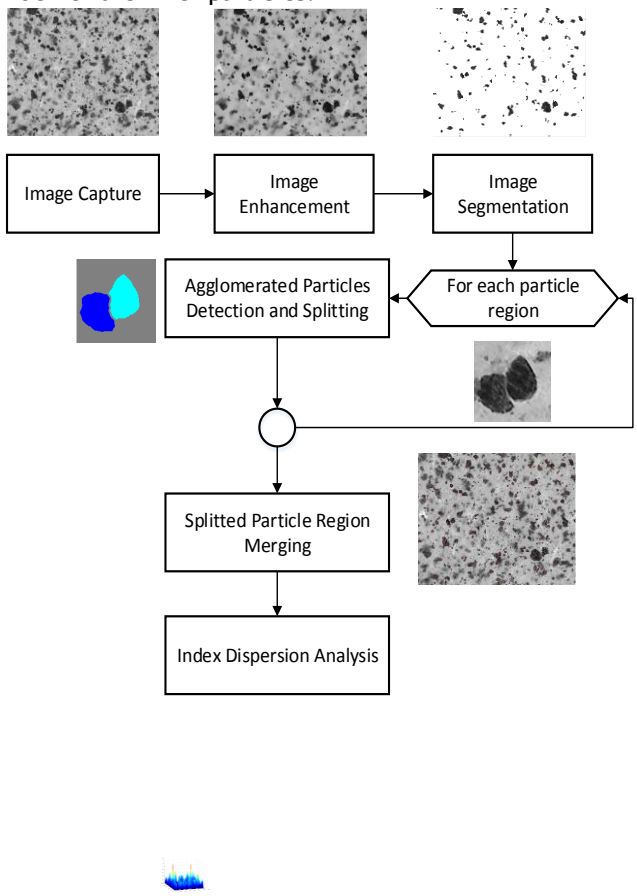

Fig. 1 Flow diagram of the filler particle dispersion analyzer

2.1. Image Enhancement Method

The algorithm used to improve the quality of the microstructure image has two stages. The first stage is enhancing dark color sharpness, which is the bottom ash particles' color. The second step is a hybrid noise reduction method, combining the spatial filter method and the multiresolution wavelet approach. The process of enhancing the image quality uses a two-dimensional input image, which is then represented by I, which has some rows M and the number of columns N. From the input image, the average grey value is calculated. Suppose it is represented by the variable μ, which is obtained by the formula:

$$\mu = \sum_{i=1}^{M}\sum_{j=1}^{N}\frac{I(i,j)}{M.N} \quad (1)$$

where i = 1,2,3, ..., M and j = 1,2,3, ..., N are the row and column coordinates of the pixels in the input image I. Then a convolution operation, as described in [22], is performed between the input image I and the average filter of 3x3 size as follows:

$$\omega = \begin{bmatrix} 1/9 & 1/9 & 1/9 \\ 1/9 & 1/9 & 1/9 \\ 1/9 & 1/9 & 1/9 \end{bmatrix}$$

which will produce an average image, I_{mean} with the following equation:

$$I_{mean}(i,j) = \sum_{dx=-1}^{1}\sum_{dy=-1}^{1}\omega(dx,dy)I(i+dx,j+dy) \quad (2)$$

where i, j is the coordinate of a pixel in the image I; dx, and dy is a distance between the center and the edge of the neighborhood window.

Furthermore, each pixel in the image Imean is selected, whose value is $<0.5\mu$ to detect dark areas of filler particles. This operation will produce a binary image, I_{bw}, with a value of 1 for the fill particle area and 0 for the area other than the fill particle area. Next, the brightness of the image Imean is decreased by multiplying each pixel by 0.5, that expressed as:

$$I'_{mean} = 0.5I_{mean} \quad (3)$$

Suppose each grey value of pixels in I_{mean} is multiplied by the binary image I_{bw}. It will produce an image with a grey value of 0.5 from the pixel value of the image Imean in the selected area called I_{select}. Meanwhile, the greyscale of the selected pixels in the input image I is taken by operating the dot product between I and the inverse of I_{bw}. This result is an image $I_{\text{nonselect}}$ that resembles the input image I but with the black particle. Moreover, finally, the grayscale of the image $I_{\text{nonselect}}$ is added to the grayscale of the image I_{select} that will result in an image with a darker particle region so that the particle will be easier to distinguish from the matrix.

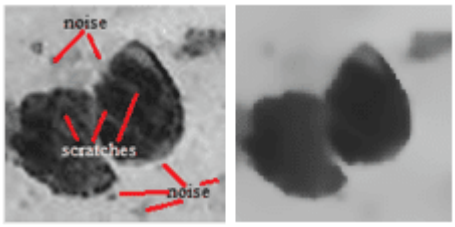

Fig. 2 Before and after noise reduction

In making polymer composites, there is a stirring, mixing, and grinding process that results in the destruction of filler particles into more delicate flakes or dust. These fragments are difficult to distinguish from dust or dirt and become noise in microscopic images, as shown in Fig. 2. So the next enhancement step aims to remove noise or small lines while maintaining the detail of the filler particle area [18] using the hybrid speckle-noise reduction method proposed by Hermawati et al. [23]. The step begins

with decomposition by applying the process, namely wavelet transformation, on the image of *n*-levels. The multiresolution wavelet approach offers advantages in eliminating noise at several levels of resolution in different image components. At each level, this decomposition process will produce one sub-image with an approximation component from the input image and three sub-images with a detailed part with horizontal, vertical, and diagonal directions. Starting from the *n*-th decomposition level, a sub-image is taken with an approximation component. This sub-image was processed using bilateral filters.

Meanwhile, the three sub-images with detailed elements at the same level were processed by soft-thresholding then processed by the anisotropic diffusion method. The process results on the four sub-images are recombined by applying an inverse wavelet transformation that will produce an approximate image at the *n*-1 level. The process is repeated until it reaches level=1.

Fig. 2 shows that noise is lost after the noise reduction process, and scratches on the lamina's surface due to treatment before image capture with a microscope can also be minimized. The noise reduction method's advantage is still preserving the object's edge to facilitate the next step's edge detection process.

2.2. Image Segmentation

After improving the processed microstructure image quality, a segmentation algorithm is performed to separate the polymer matrix area's filler particle area. We applied the fuzzy entropy-based multi-level thresholding method proposed by Sarkar et al. [18] to obtain the filler area layers. This method will segment the input image's grayscale as much as *n*-level starting from the darkest color (black) to the lightest color (white). Suppose the image *I* is segmented in *n*-level segments, the threshold value *T* at level *i* is defined as:

$$T_i = \frac{lb_i + ub_{i-1}}{2} \quad (4)$$

where lb_i is the lower bound of trapezoidal fuzzy membership function for *i*-segment and ub_i-1 is the upper bound of trapezoidal fuzzy membership function for the *i*-1 segment.

The filler particles in the form of bottom ash on the surface (first layer) of the matrix will have the darkest color and will fade become grey if it is in the matrix's base layer. In contrast, the color of the matrix tends to be bright or whitish. By applying this multi-level thresholding method, for example, with $n = 4$ as shown in Fig. 3(a), we will get four areas with different grey levels. They are the brightest matrix area, the deepest filler particle layer, the filler on the second layer, and the filler particle layer located in the uppermost layer (surface). At this stage, the particle area will be processed in different layers starting from the top layer. From each layer, a binary image with a value of 1 is the particle area. Fig. 3(b) presents a binary image for particle area in the surface layer.

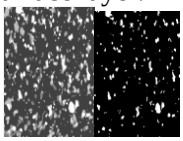

(a) (b)

Fig. 3 (a) Segmented regions for number level = 4; (b) Segmented particle region in the surface layer

2.3. Agglomerated Particle Splitting

After the segmentation process, for each particle area in the binary image, the detection and separation of clumped or stacked particles are carried out. Stacked areas are indicated by the size of the particle area that is greater than 500 pixels. The bounding box of the particle area in the binary image plus 20 pixels on the left, top, right, and bottom is used as a mask to get the particle area in the input image.

The procedure for separating and identifying the agglomerating particles consists of several steps, as shown in Fig. 4. The first step is to improve particle image quality using the image enhancement algorithm. This step is to smooth and to level grey values in the particle area. The splitting process's primary stage begins with the edge detection process to get the particle boundary's shape. The next step is the gap-filling to get the edge lines that separate the regions in the clumping particle image. The splitting area has obtained by the difference between the hole filling area of the boundary and the boundary itself.

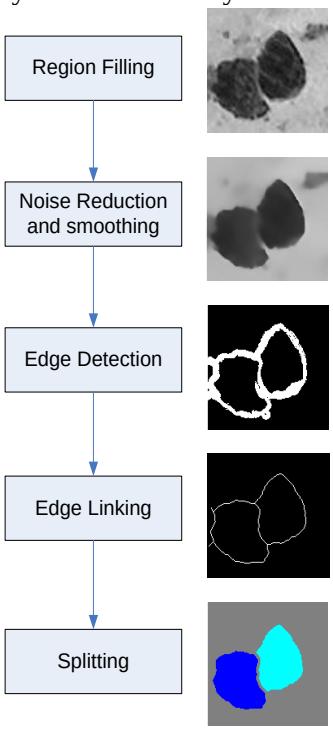

Fig. 4 Block diagram of the proposed segmentation method for particle splitting

2.3.1. Region Filling

The first step is region filling. Proper preliminary processing is needed to improve the accuracy of the particle filler fillings of these polymer composites. One of the problems is the presence of voids on the lamina's

surface. It is due to the air being captured in the process of lamina making. These voids are usually brighter areas in the microscopic image of the lamina's surface with sizes that can be small and can be large, as can be seen in the example in Fig. 5(a). If there is a void on the layer of particles that will be detected, it will cause holes in the segmentation results, as in Fig. 5(b), so that the results of segmentation become imperfect.

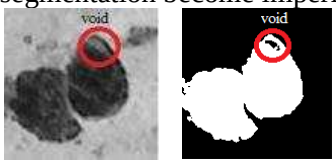

(a) (b)

Fig. 5 (a) Void in a grayscale image; (b) Void in a binary image

The region filling is used to fill the void area with a grey value similar to its neighbors' average intensities — the outline of the region filling steps as in Fig. 6. The region filling process begins with thresholding to obtain the area of the filling particles. The threshold value to get a binary image is equal to the maximum grey level value minus the minimum grey level value, divided by two. The holes in the particle area in the thresholding result's binary image are filled using the hole filling method. A mask can be obtained by subtracting the hole filling results with the thresholding results. The dilation process uses a 3x3 square structuring element to get the hole's intensities in the mask image. Furthermore, the average of grayscales in the mask area obtained in the input image is used to replace the mask area's grey value.

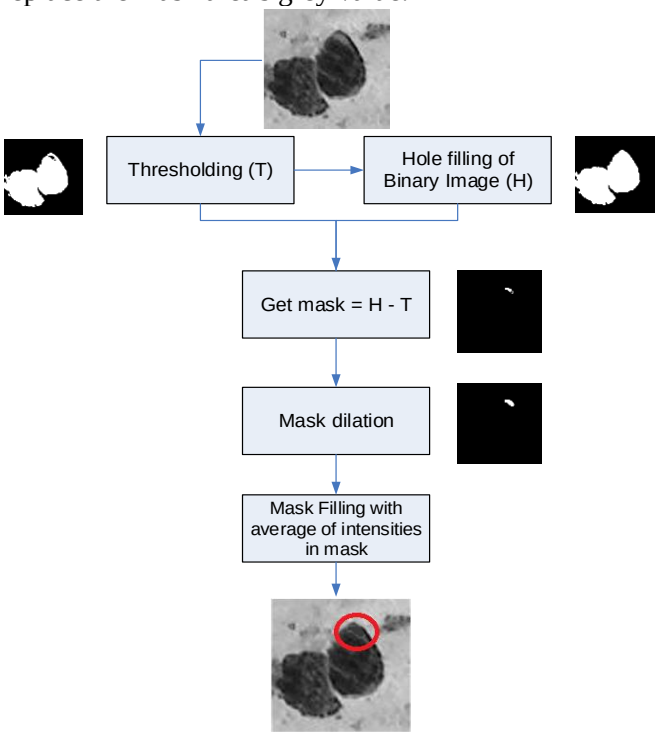

Fig. 6 Block diagram of the region filling step

2.3.2. Edge Detection

The edge detection step is used to get the boundary of objects and the borderline between overlapping items. There are several types of operators used in edge detection, including Canny, Prewitt, and Sobel. In their research, Muhammad Umair et al. [24] used the Canny operator to detect rough sea horizon lines. However, in this study, we apply the Prewitt operator since it does not require two threshold values like the Canny operator. The Prewitt operator is used to get the first derivative image in the horizontal direction and vertical direction. The edge image is obtained from the two derivatives' magnitudes that meet specific threshold values, as shown in Fig. 7(a). The magnitude image with a dark background contains non-zero grey level values, which are the image's edges. By taking a grey level value that is greater than the threshold, we will get an edge image as in Fig. 7(b).

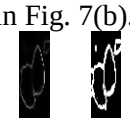

(a) (b)

Fig. 7 The magnitude image and the thresholding result

After obtaining the edge image, removing unwanted objects outside the particle objects will be separated in the image. The process can be carried out using the 'open' morphological operator to eliminate objects smaller than the specified size threshold, for example, objects smaller than 900 pixels. Another way is to select an object with the most significant area property.

2.3.3. Edge Linking

The edge linking process connects pixels in the edge image to get a boundary line from the object. It is a process to fill a small gap that might occur at the edge image. The gap pixels are zero values that appear between the value of one in the edge image, as in Fig. 8.

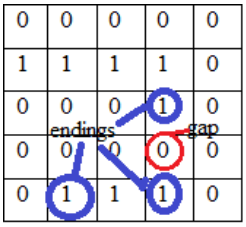

Fig. 8 Gap and ending pixels of the edge image

The algorithm of the gap-filling process can be seen in the flowchart of Fig. 9. Firstly, we have to find the pixels at the end of the line by checking the number of transitions or crossings between zero and one of the neighbors, measuring 3x3 each edge pixel. Furthermore, a pixel at the end of the line, a circular mask is placed. The mask has a radius equal to the gap of 1 divided by 2. The final step of the gap-filling process is to carry out a thinning process to get the resulting line.

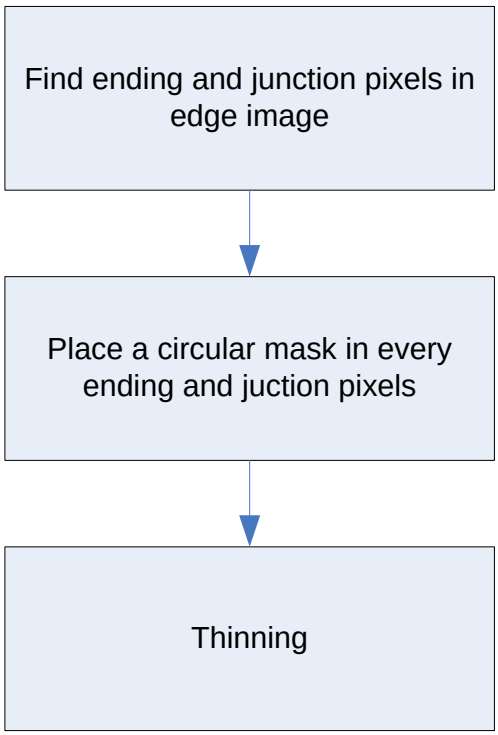

Fig. 9 Gap connection process

2.3.4. Splitting

After the edge's connecting process is carried out, the next step is to separate between two or more areas bounded by the edge lines. The stages of separation can be seen in Fig. 10. Firstly, we apply a Gaussian filter to smooth the edge image. The smoothing process aims to ease and widen the line and fill gaps at the previous stage. After that, we implement the thresholding step to get the binary image from the smoothed edge image with the threshold value is equal to zero. The hole filling process is used to obtain the whole particle area. The difference between the entire particle area and the edge image will result in the splitting region.

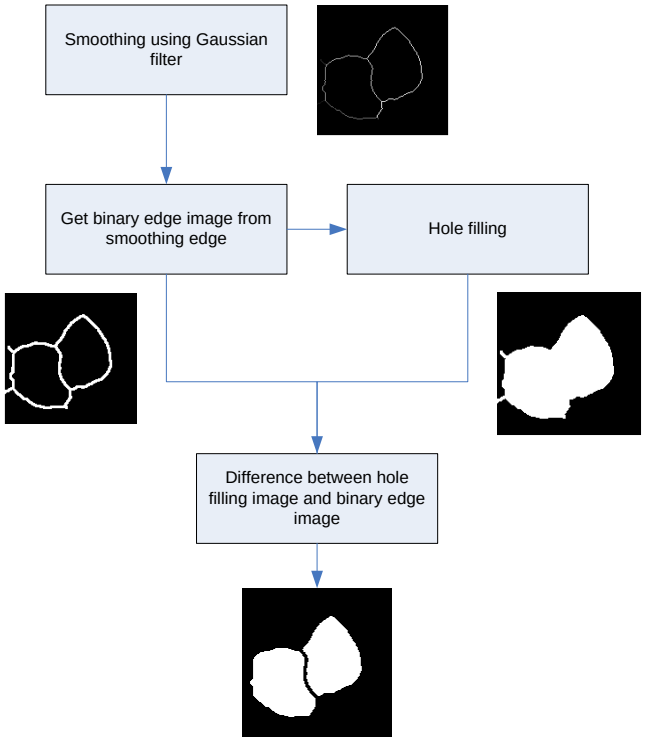

Fig. 10 Block diagram of splitting step

2.4. Index Dispersion Analysis

After all particle areas in one layer have been processed, incorporation and detection of the particle center are performed. The separated particle areas are then recombined to the position of the particle in the original image. Then look for the center point of each particle area. The particle center point information is used in the last step to calculate the dispersion index. The mean distance between the center points of the particles in the image is calculated. It is the dispersion index, which shows the degree of distribution of the filler particles in the polymer matrix, which is expressed as [8]:

$$\boldsymbol{d_{L2}(G,U)} = \sqrt{\sum_{x=1}^{M}(\boldsymbol{G(x)} - \boldsymbol{U(x)})^2} \quad (5)$$

U(x) is a function of uniform distribution of pixels in the input image; G(x) is a normal distribution expressed as the particle center points' Gaussian density function. *M* is the spatial resolution of the input image.

3. Results and Discussion

3.1. Data Collection

The materials needed for the manufacture of composite polymers are thermoplastic polymers (polypropylene) and coal ash with 200 and 250 mesh with a concentration of 2% and 5%. Polypropylene polymer, which has been weighed with a certain weight, is put into a container (stirrer) heating, heated to a temperature of 170^{o}C. This temperature corresponds to the melting temperature of polypropylene. After 100% melting, which takes almost 2 hours to weigh 300 grams of polypropylene, a weighted coal ash powder is added and has a specific mesh particle size. After all the fillers have entered, stir for 30 minutes at a certain speed. The composite material mixture is ready to be printed into a rectangular mold, 10 mm thick, 20 mm wide, and 200 mm long after the mixing. With a pressure of 20 kg / mm2, and let stand for 5 minutes. After cooling, the composite material is ready to be removed from the mold.

Microstructural images were obtained from composite sheets (lamina), which had a bottom ash content of 2% and 5% by weight of the mixture using a Dino-lite digital microscope with minimal magnification 60 times. Fig. 11 shows that the bottom ash particle has a dark color, and the polypropylene matrix has a brighter color. Fig. 11 also shows the bottom ash particle's position in the surface layer and spread in the deeper layers indicated by different grey levels. The farther from the observation's surface, the greyscale of the bottom ash is larger or brighter. The

samples of agglomeration bottom ash image can be seen in Fig. 12. In the experiment for the agglomeration particle segmentation method, we used 121 images of filler particles.

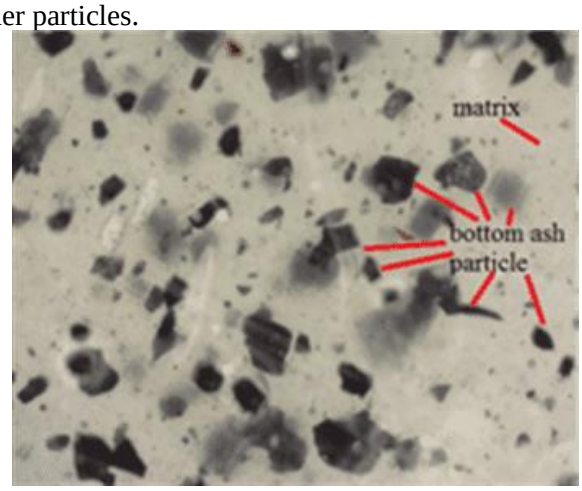

Fig. 11 Microstructure image of polymer composite reinforced by bottom ash particles

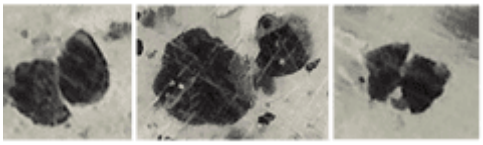

Fig. 12 Sample of the agglomeration particle

3.2. Performance Evaluation

To measure the proposed splitting algorithm's performance, we implemented the region-based performance measurements, i.e., precision as in Equation 6, accuracy as in Equation 9, sensitivity as in Equation 7, specificity as in Equation 8, and Dice similarity as in Equation 10. Region-based metrics, as defined in [25], were chosen as a way to assess the precision and accuracy of different segmentation methods for splitting the agglomerative particle. For example, R_{SR} shows the segmentation results region, and R_{GT} is the ground truth described by experts. All area-based metrics are given as percentages, i.e.

1. Precision P is the accuracy of experts' segmentation results with the system's segmentation results. P characterizes the number of regions that is common in both R_{SR} and R_{GT} divided by the total number of area in the combined R_{SR} and R_{GT} as follows:

$$P = \frac{\left|R_{SR} \cap R_{GT}\right|}{\left|R_{SR} \cup R_{GT}\right|} \tag{6}$$

2. Accuracy is defined as the closeness level between the segmentation result and the actual region assessed by the True Positive (TP) and True Negative (TN) calculation of each method. True Positive Rate (TPR) is the quotient of the total number of the actual area that is covered by the segmentation technique and represents delineation sensitivity, defined as:

$$TPR = \frac{\left|R_{SR} \cap R_{GT}\right|}{\left|R_{GT}\right|} \tag{7}$$

True Negative Rate (TNR) is the quotient of the total area in the reference region that is not the actual area and excluded from the segmented area. It states the delineation specificity and is defined as:

$$TNR = \frac{\left|(R_{SR} \cup R_{GT})^c\right|}{\left|(R_{GT})^c\right|} \tag{8}$$

where $(.)^c$ shows the complement of a reference region set. From both *TP* and *TN*, measurements accuracy can be calculated with the following equation:

$$Acc = \frac{|TP| + |TN|}{|O_{GT}| + |(O_{GT})^c|} \tag{9}$$

3. Dice similarity *D* provide indications of overlapping between R_{SR} and R_{GT} that is defined as follow:

$$D = \frac{2\left|R_{SR} \cap R_{GT}\right|}{\left|R_{GT}\right| + \left|R_{SR}\right|} \tag{10}$$

3.3. Experiments

In this section, we will present the result and performance of our proposed method. The research results' scope includes the results of the image enhancement method, the performance of the proposed particle splitting method, and the results of filler dispersion quantification.

Firstly, we compared the segmentation result with our enhancement technique versus without the enhancement step, as shown in Fig. 13. Fig. 13(b) presents the input image's enhancement result in Fig. 13(a). Fig. 13(c) and Fig. 13(d) are the segmented image of the original image in Fig. 13(a) and the segmented image of the enhanced image in Fig. 13(b), respectively. As shown in Fig. 13(c), the segmentation results without the enhancement process resulted in an incomplete particle area, which would complicate the next step's dispersion analysis process.

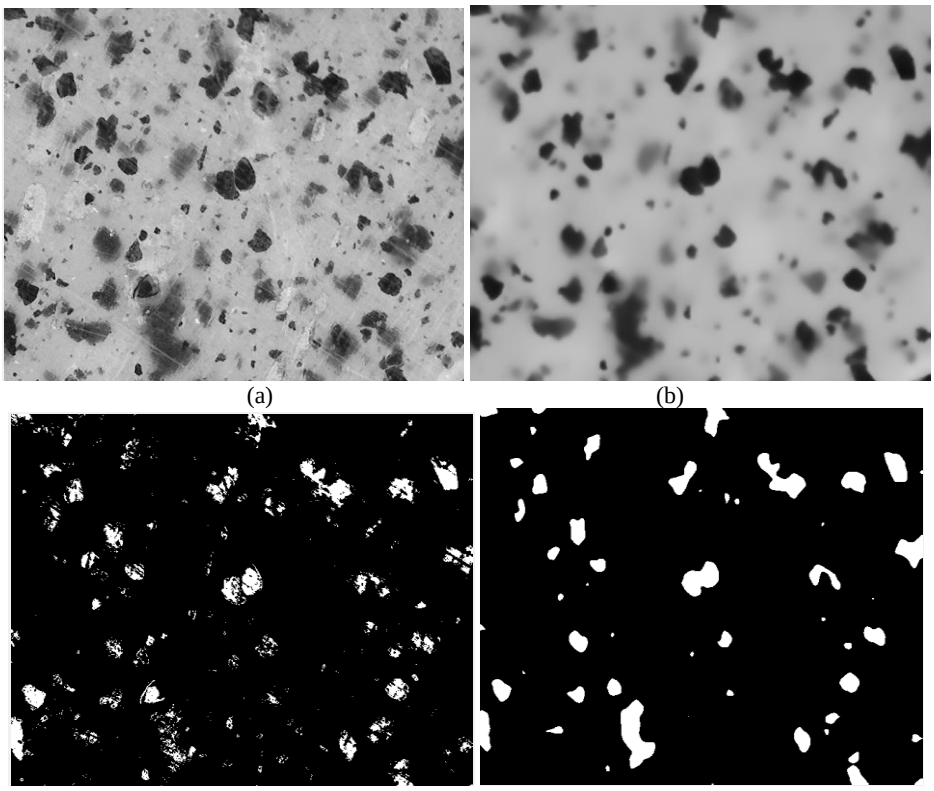

(a) (b)

(c) (d)

Fig. 13 (a) Image input; (b) Enhanced image; (c) Segmentation result of image input; (d) Segmentation result of enhanced image

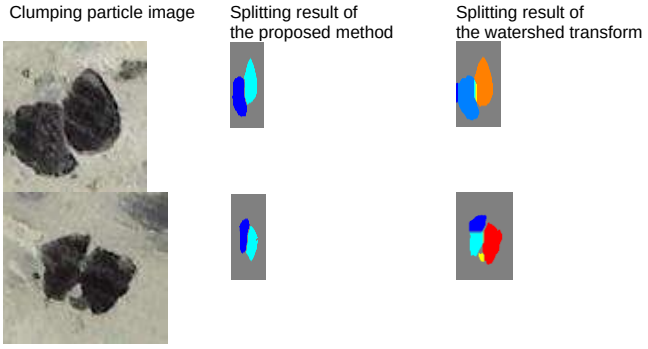

Fig. 14 Comparison of the splitting particle result

Next, we compare the performance of our proposed particle splitting method with the watershed method [14]. In this study, we set the parameter for the threshold of edge detection is equal to 8, the gap size is the same as 5, the Gaussian filter size is 3x3 with a standard deviation of 0.2. The example of segmentation results using the proposed method and the watershed method is presented in Fig. 14. From Fig. 14, we can see that the proposed method more precise than the watershed method.

Table 1 Average of performance measurement

Measurement	**Proposed Method**	**Watershed Method**
Precision	0.824	0.726
Accuracy	0.910	0.857
Sensitivity	0.840	0.765
Specificity	0.980	0.948
Dice similarity	0.902	0.817

Table 1 shows that overall, the performance of the proposed segmentation method for particle splitting is better than the watershed method, where the accuracy of the proposed method reaches 91%. For segmentation of objects with irregular shapes as in this study, the proposed method also gives a reasonably high precision value of 82.4% and a sensitivity that indicates a sufficiently high level of True Positive that reaches 84%. This distinctive depiction achieves 98%, which means that segmentation results are mostly in the ground truth area. This value shows that the size of the segmented area is smaller than the ground truth area. In contrast, the common overlapping area between the segmentation area and the ground truth area reaches 90.2%.

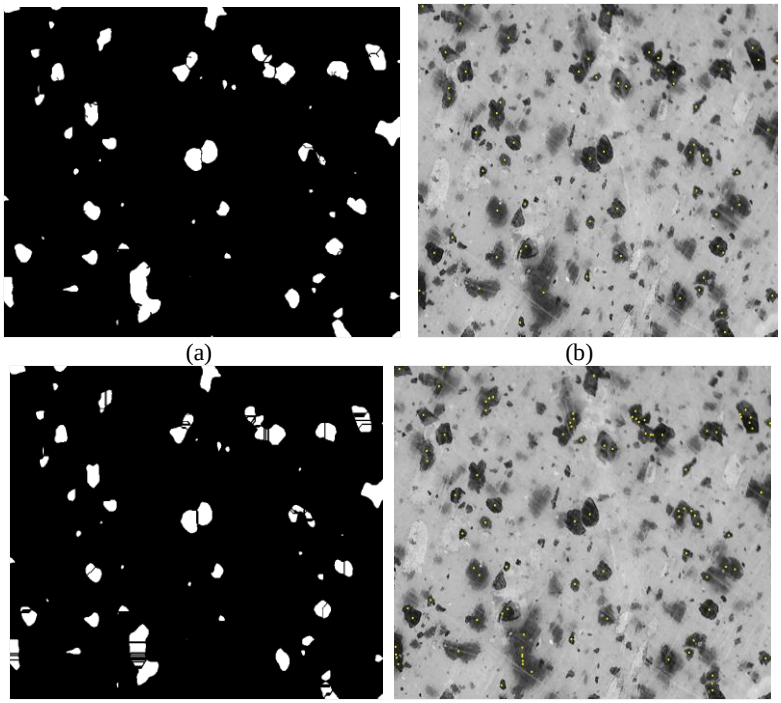

Fig. 15 (a) Splitting result using proposed method; (b) Particles distribution using the proposed method; (c) Splitting result using watershed method; (d) Particles distribution using the watershed method

Finally, we compared all particles' segmentation results in the whole image after the splitting process and the particles' distribution. Fig. 15 present the comparison of the segmentation result with our proposed splitting method and watershed method. As we know that the watershed method uses the principle of measuring the distance from the edge of the object to the center, where the object's center is determined using a distance transformation. It will produce multiple centers if the object's shape is asymmetrical or irregular, as in our problem. This property will cause over-segmentation and cause particles not to separate according to the actual particle shape, as shown in Fig. 15(c). So that in the analysis of particle distribution, it will cause a high number of particles in the splitting area using the watershed method. Meanwhile, our proposed method can separate particles according to their shape because we apply an edge detection-based approach, as present in Fig. 15(a).

4. Conclusion

An automatic method for detecting and analyzing the filler particle distribution using image processing techniques was successfully applied in the bottom ash reinforced polymer composite. The image enhancement was conducted to improve particle sharpness and remove noises with the same properties as the particles. Implementation of the image enhancement can ease the particle analysis at the following step. The particle splitting algorithm had a better performance than the watershed method, with an accuracy of 91%, sensitivity 84%, specificity 98%, and dice similarity of 90.2%. In practice, the proposed method could quantize the filler particle dispersion in a matrix to find out the polymer composite material's strength easily and faster.

This method's drawback is that the segmented area's size is smaller than the actual area, likely the thinning process at the gap joining stage. For this reason, it is necessary to develop a better method of connecting holes without reducing the size of the area produced. Also, it is required to establish a method for evaluating the material's strength based on the particle distribution calculation in the future.

Acknowledgments

This research was funded by the Higher Education Leading Applied Research (PTUPT) from The Ministry of Research, Technology & Higher Education of the Republic of Indonesia based on grant number: 229/SP2H/LT/DRPM/2019 dated March 11, 2019, and contract number: 407/02/AMD/003/LPPM/Lit/V1 /2020.

References

[1] NGO T.-D. Introduction to Composite Materials. In: NGO T.-D. (ed.) *Composite and Nanocomposite Materials: From Knowledge to Industrial Applications*. IntechOpen, 2020: 1–27. https://doi.org/10.5772/intechopen.91285

[2] ANANE-FENIN K., AKINLABI E.T., and PERRY N. Quantification of nanoparticle dispersion within polymer matrix using gap statistics. *Materials Research Express*, 2019, 6: 075310. https://doi.org/10.1088/2053-1591/ab1106

[3] KARASINSKI E. D. N., SASSE F. D., and COELHO L. A. F. Multifractal analysis of particle dispersion and interphase percolation in nanocomposites. *Materials Research*, 2018, 21(5): e20180265. https://doi.org/10.1590/1980-5373-mr-2018-0265

[4] SANTOS R. M., MOULD S. T., FORMÁNEK P., PAIVA M. C., and COVAS J. A. Effects of particle size and

surface chemistry on the dispersion of graphite nanoplates in polypropylene composites. *Polymers*, 2018, 10(2): 222. https://doi.org/10.3390/polym10020222
[5] ZACCARDI F., SANTONICOLA M. G., and LAURENZI S. Quantitative assessment of nanofiller dispersion based on grayscale image analysis: A case study on epoxy/carbon nanocomposites. *Composites Part A: Applied Science and Manufacturing*, 2018, 115: 302–310. https://doi.org/10.1016/j.compositesa.2018.10.003
[6] WANG G., YU D., KELKAR A. D., and ZHANG L. Electrospun nanofiber: Emerging reinforcing filler in polymer matrix composite materials. *Progress in Polymer Science*, 2017, 75: 73–107. https://doi.org/10.1016/j.progpolymsci.2017.08.002
[7] MARTINEZ R. F., ITURRONDOBEITIA M., IBARRETXE J., and GURAYA T. Methodology to classify the shape of reinforcement fillers: optimization, evaluation, comparison, and selection of models. *Journal of Materials Science*, 2017, 52: 569–580. https://doi.org/10.1007/s10853-016-0354-1
[8] LI Z., GAO Y., MOON K.-S., YAO Y., TANNENBAUM A., and WONG C. P. Automatic quantification of filler dispersion in polymer composites. *Polymer*, 2012, 53: 1571–1580. https://doi.org/10.1016/j.polymer.2012.01.048
[9] RAMZI N. I. R., SHAHIDAN S., MAAROF M. Z., and ALI N. Physical and Chemical Properties of Coal Bottom Ash (CBA) from Tanjung Bin Power Plant. *IOP Conference Series: Materials Science and Engineering*, 2016, 160: 012056. https://doi.org/10.1088/1757-899X/160/1/012056
[10] KASTIAWAN I. M., SUTANTRA I. N., and SUTIKNO. Correlation of Holding Time and Bottom Ash Particle Size to Mechanical Properties of Polypropylene Composite. *Key Engineering Materials*, 2020, 867: 172–181. https://doi.org/10.4028/www.scientific.net/kem.867.172
[11] KASTIAWAN I. M., SUTANTRA I. N., and SUTIKNO S. Effect of Bottom Ash Treatment and Process Variables on the Strength of Polypropylene Composites. *International Review of Mechanical Engineering*, 2020, 14: 324. https://doi.org/10.15866/ireme.v14i5.18804
[12] ESCHWEILER D., SPINA T. V., CHOUDHURY R. C., MEYEROWITZ E., CUNHA A., and STEGMAIER J. CNN-Based Preprocessing to Optimize Watershed-Based Cell Segmentation in 3D Confocal Microscopy Images. Proceedings of the IEEE 16th International Symposium on Biomedical Imaging, Venice, 2019, pp. 223–227. https://doi.org/10.1109/isbi.2019.8759242
[13] ARIS T. A., NASIR A. S. A., and MUSTAFA W. A. Analysis of distance transforms for watershed segmentation on chronic leukaemia images. *Journal of Telecommunication, Electronic and Computer Engineering*, 2018, 10: 51–56. https://journal.utem.edu.my/index.php/jtec/article/view/4074
[14] ZHANG Y., & XU D. Improved watershed algorithm for cell image segmentation. *Advanced Materials Research*, 2012, 546–547: 464–468. https://doi.org/10.4028/www.scientific.net/AMR.546-547.464
[15] KORNILOV A. S., & SAFONOV I. V. An overview of watershed algorithm implementations in open source libraries. *Journal of Imaging*, 2018, 4(10): 123. https://doi.org/10.3390/jimaging4100123
[16] JI X. Q., LI Y., CHENG J. Z., YU Y., and WANG M. Cell image segmentation based on an improved watershed algorithm. Proceedings of the 8th International Congress on Image and Signal Processing, Shenyang, 2015, pp. 433–437. https://doi.org/10.1109/CISP.2015.7407919
[17] KOWAL M., ŻEJMO M., SKOBEL M., KORBICZ J., and MONCZAK R. Cell Nuclei Segmentation in Cytological Images Using Convolutional Neural Network and Seeded Watershed Algorithm. *Journal of Digital Imaging*, 2020, 33: 231–242. https://doi.org/10.1007/s10278-019-00200-8
[18] HERMAWATI F. A., KASTIAWAN I. M., and MUHYIN. Digital Microscopy Image Enhancement Technique for Microstructure Image Analysis of Bottom Ash Particle Polymer Composites. In: PARINOV I., CHANG S. H., and LONG B. (eds.) *Advanced Materials. Springer Proceedings in Materials*, Vol. 6. Springer, Cham, 2020: 235–244. https://doi.org/10.1007/978-3-030-45120-2_20
[19] SARKAR S., PAUL S., BURMAN R., DAS S., and CHAUDHURI S. S. A Fuzzy Entropy Based Multi-Level Image Thresholding Using Differential Evolution. In: PANIGRAHI B., SUGANTHAN P., and DAS S. (eds.) *Swarm, Evolutionary, and Memetic Computing. SEMCCO 2014. Lecture Notes in Computer Science*, Vol. 8947. Springer, Cham, 2015: 386–395. https://doi.org/10.1007/978-3-319-20294-5_34
[20] NAIDU M. S. R., KUMAR P. R., and CHIRANJEEVI K. Shannon and Fuzzy entropy based evolutionary image thresholding for image segmentation. *Alexandria Engineering Journal*, 2018, 57: 1643–1655. https://doi.org/10.1016/j.aej.2017.05.024
[21] HERMAWATI F. A., TJANDRASA H., SUGIONO, SARI G. I. P., and AZIS A. Automatic femur length measurement for fetal ultrasound image using localizing region-based active contour method. *Journal of Physics: Conference Series*, 2019, 1230: 012002. https://doi.org/10.1088/1742-6596/1230/1/012002
[22] SOMAWIRATAA I. K., WIDODOA K. A., ACHMADIA S., and UTAMININGRUM F. Road Detection Based on Statistical Analysis. *Journal of Hunan University Natural Sciences*, 2020, 47(12): 57–64. http://jonuns.com/index.php/journal/article/view/487
[23] HERMAWATI F. A., TJANDRASA H., and SUCIATI N. Hybrid Speckle Noise Reduction Method for Abdominal Circumference Segmentation of Fetal Ultrasound Images. *International Journal of Electrical and Computer Engineering*, 2018, 8: 1747–1757. http://doi.org/10.11591/ijece.v8i3.pp1747-1757
[24] UMAIR M., HASHMANI M. A., and KEIICHI H. Rough-Sea-Horizon-Line Detection using a Novel Color Clustering and Least Squares Regression Method. *Journal of Hunan University Natural Sciences*, 2020, 47(12): 133–145. http://jonuns.com/index.php/journal/article/view/491
[25] UDUPA J. K., LEBLANC V. R., ZHUGE Y., IMIELINSKA C., SCHMIDT H., CURRIE L. M., HIRSCH B. E., and WOODBURN J. A Framework for Evaluating Image Segmentation Algorithms. *Computerized Medical Imaging and Graphics*, 2006, 30: 75–87. https://doi.org/10.1016/j.compmedimag.2005.12.001

参考文:

[1] 非政府组织T.-D。复合材料简介。在：非政府组织T.-D.（编。）复合材料和纳米复合材料：从知识到工业应用。英泰公开赛，2020：1-

27。https://doi.org/10.5772/intechopen.91285

[2] ANANE-FENIN K.，AKINLABI E.T. 和 PERRY N. 使用间隙统计量定量分析聚合物基质中的纳米颗粒分散体。材料研究快报，2019，6：075310. https://doi.org/10.1088/2053-1591/ab1106

[3] KARASINSKI E. D. N.，SASSE F. D. 和 COELHO L. A. F. 纳米复合物中颗粒分散和相间渗滤的多重分形分析。材料研究，2018，21（5）：e20180265。https://doi.org/10.1590/1980-5373-mr-2018-0265

[4] SANTOS R. M.，MOLD S. T.，FORMÁNEKP.，PAIVA M. C. 和 COVAS J. A. 粒度和表面化学性质对聚丙烯复合材料中石墨纳米板分散性的影响。聚合物，2018，10（2）：222. https://doi.org/10.3390/polym10020222

[5] ZACCARDI F.，SANTONICOLA M. G. 和 LAURENZI S. 基于灰度图像分析的纳米填料分散体的定量评估：环氧/碳纳米复合材料的案例研究。复合材料A部分：应用科学与制造，2018，115：302-310。https://doi.org/10.1016/j.compositesa.2018.10.003

[6] 王刚，于丹，凯尔卡·A·德 和 张力。电纺纳米纤维：聚合物基复合材料中新兴的增强填料。高分子科学进展，2017，75：73-107。https://doi.org/10.1016/j.progpolymsci.2017.08.002

[7] MARTINEZ R. F.，ITURRONDOBEITIA M.，IBARRETXE J. 和 GURAYA T. 对增强填料形状进行分类的方法：优化，评估，比较和模型选择。材料科学学报，2017，52：569-580。https://doi.org/10.1007/s10853-016-0354-1

[8] LI Z.，GAO Y.，MOON K.-S.，YAO Y.，TANNENBAUM A. 和 WONG C. P。聚合物复合物中填料分散的自动定量。聚合物，2012，53：1571-1580。https://doi.org/10.1016/j.polymer.2012.01.048

[9] RAMZI N. I. R.，SHAHIDAN S.，MAAROF M. Z. 和 ALI N. 丹戎宾电厂的煤灰（CBA）的理化性质。IOP会议系列：材料科学与工程，2016，160：012056. https://doi.org/10.1088/1757-899X/160/1/012056

[10] KASTIAWAN I. M.，SUTANTRA I. N. 和 SUTIKNO。保持时间和底灰粒度与聚丙烯复合材料力学性能的相关性。关键工程材料，2020，867：172-181。https://doi.org/10.4028/www.scientific.net/kem.867.172

[11] KASTIAWAN I. M.，SUTANTRA I. N. 和 SUTIKNO S. 底灰处理和工艺变量对聚丙烯复合材料强度的影响。机械工程国际评论，2020，14：324. https://doi.org/10.15866/ireme.v14i5.18804

[12] ESCHWEILER D.，SPINA T. V.，CHOUDHURY R. C.，MEYEROWITZ E.，CUNHA A. 和 STEGMAIER J. 基于有线电视新闻网的预处理可优化3D共聚焦显微镜图像中基于分水岭的细胞分割。电气工程师学会第16届国际生物医学成像研讨会论文集，威尼斯，2019，第 223–227 页。https://doi.org/10.1109/isbi.2019.8759242

[13] ARIS T. A.，NASIR A. S. A. 和 MUSTAFA W. A. 在慢性白血病图像上进行分水岭分割的距离变换分析。电信，电子与计算机工程学报，2018，10：51-56。https://journal.utem.edu.my/index.php/jtec/article/view/4074

[14] ZHANG Y.，和 XU D. 改进的分水岭算法用于细胞图像分割。先进材料研究，2012，546-547：464-468。https://doi.org/10.4028/www.scientific.net/AMR.546-547.464

[15] KORNILOV A. S. 和 SAFONOV I. V. 开源库中分水岭算法实现的概述。影像学杂志，2018，4（10）：123. https://doi.org/10.3390/jimaging4100123

[16] 季新启，李Y，程建中，于Y，和 王敏。一种基于改进分水岭算法的细胞图像分割。第八届国际图像和信号处理大会论文集，沉阳，2015，第 433-437 页。https://doi.org/10.1109/CISP.2015.7407919

[17] KOWAL M.，EJMO M.，SKOBEL M.，KORBICZ J. 和 MONCZAK R. 使用卷积神经网络和种子分水岭算法在细胞学图像中进行细胞核分割。数字影像杂志，2020，33：231-242。https://doi.org/10.1007/s10278-019-00200-8

[18] HERMAWATI F. A.，KASTIAWAN I. M. 和 MUHYIN。底灰颗粒聚合物复合材料微结构图像分析的数字显微镜图像增强技术。在：PARINOV I.，CHANG S. H. 和 LONG B.（编辑）先进材料中。斯普林格材料学报，第一卷。6.查纳·施普林格，2020：235–244。https://doi.org/10.1007/978-3-030-45120-2_20

[19] SARKAR S.，PAUL S.，BURMAN R.，DAS S. 和 CHAUDHURI S. S. 基于微分演化的基于模糊熵的多级图像阈值。在：PANI GRAHI B.，SUGANTHAN P. 和 DAS S.（编辑）群，进化和模因计算中。胜科2014。计算机

科学讲义，第1卷。8947。施普林格，湛，2015：386-395。https://doi.org/10.1007/978-3-319-20294-5_34

[20] NAIDU M. S. R.，KUMAR P. R. 和 CHIRANJEEVI K.
香农和基于模糊熵的进化图像阈值用于图像分割。亚历山大工程学报，2018，57：1643-1655。https://doi.org/10.1016/j.aej.2017.05.024

[21] HERMAWATI F. A.，TJANDRASA H.，SUGIONO，SARI G. I. P. 和 AZIS A。使用基于局部区域的主动轮廓法自动测量胎儿超声图像的股骨长度。物理学杂志：会议系列，2019，1230：012002. https://doi.org/10.1088/1742-6596/1230/1/012002

[22] SOMAWIRATAA I. K.，WIDODOA K. A.，ACHMADIA S. 和 UTAMININGRUM F. 基于统计分析的道路检测。湖南大学学报（自然科学版），2020，47（12）：57-64。http://jonuns.com/index.php/journal/article/view/487

[23] HERMAWATI F. A.，TJANDRASA H. 和 SUCIATI N. 混合斑点噪声降低方法用于胎儿超声图像的腹部围壁分割。国际电气与计算机工程杂志，2018，8：1747–1757。http://doi.org/10.11591/ijece.v8i3.pp1747-1757

[24] UMAIR M.，HASHMANI M. A. 和 KEIICHI H. 使用新颖的颜色聚类和最小二乘回归方法进行的海平面地平线检测。湖南大学学报（自然科学版），2020，47（12）：133-145。http://jonuns.com/index.php/journal/article/view/491

[25] UDUPA J. K.，LEBLANC V. R.，ZHUGE Y.，IMIELINSKA C.，SCHMIDT H.，CURRIE L. M.，HIRSCH B. E. 和 WOODBURN J. 一种评估图像分割算法的框架。计算机医学影像与图形，2006，30：75-87。https://doi.org/10.1016/j.compmedimag.2005.12.001